LAWRENCE
LIVERMORE
NATIONAL
LABORATORY

UCRL-JRNL-215487

Reconstruction of Quasi-Monochromatic Images for Multispectral X-ray Imaging with a Pinhole Array and a Flat Bragg Mirror

N. Izumi, T. W. Barbee, J. A. Koch, R. C. Mancini, L. A. Welser

September 19, 2005

Review of Scientific Instruments

Reconstruction of Quasi-Monochromatic Images for Multispectral X-ray Imaging with a Pinhole Array and a Flat Bragg Mirror

N. Izumi[1], T. W. Barbee[1], J. A. Koch[1], R. C. Mancini[2], L. A. Welser[2],

[1]*University of California, Lawrence Livermore National Laboratory, P.O. Box 808, Livermore CA, 94550 USA*

[2]*Department of Physics, University of Nevada, Reno NV 89557, USA*

Abstract

We have developed a software package for reconstruction of quasi-monochromatic images from a multiple monochromatic x-ray imager for inertial confinement fusion implosions. The instrument consists of a pinhole array, a multi-layer Bragg mirror, and a image detector. The pinhole array projects hundreds of images onto the detector after reflection off the multi-layer Bragg mirror, which introduces spectral dispersion along the reflection axis. The quasi-monochromatic images of line emissions and continuum emissions can be used for measurement of temperature and density maps of implosion plasmas. In this paper, we describe a computer-aided processing technique for systematic reconstruction of quasi-monochromatic images from raw data. This technique provides flexible spectral bandwidth selection, and allows systematic subtraction of continuum emission from line emission images.

PACS number(s): 52.57.-Z, 52.70.La

I. INTRODUCTION

It is possible to measure electron temperatures and densities in the compressed core region of inertial confinement fusion (ICF) plasmas from measurements of the x-ray line emission from Ar dopants [1]. It is also possible to measure the areal density (ρR) of the pusher region by measuring x-ray transmission through a high-Z doped layer [2]. Spatial profiles of quasi-monochromatic x-ray emission are fundamental to understanding these physical conditions. Three methods of quasi-monochromatic X-ray imaging have been developed. The first approach is imaging with bent Bragg mirrors [3], the second approach is imaging with a Kirkpatrick-Baez microscope [4], and the third approach is a pinhole array coupled to a flat Bragg mirror [5]. One advantage of the multi-pinhole Bragg mirror approach is flexible post-processing capability. Because the multi-pinhole Bragg mirror system provides continuous coverage over a wide spectral range, various quasi-monochromatic images in different spectral regions (Ar Ly-α, Ar Ly-β, Ar He-α, Ar He-β, Ti K absorption line, and continuum emission in the vicinity of the line emission) can be constructed in software. The continuous spectral dispersion of the Bragg mirror also allows for spectral bandwidth selection in the reconstruction process. Once an appropriate bandwidth for each spectral range is selected, background components from continuum and satellite emissions can be subtracted from line emission images.

Development of a post-processor code is crucial for the systematic reconstruction of quasi-monochromatic images. Previously, Welser *et al.* developed an image-reconstruction software package for the Multiple Monochromatic Imager (MMI) [6]. This software locates, aligns, and sums individual pinhole images within the vertical extent of the raw data corresponding to the spectral region of interest. Therefore, the selected

spectral width must be larger than the image size (~ 800 μm on the detector, corresponding to a spectral width of 0.16 angstroms), and the quasi-monochromatic images are constructed with a relatively wide spectral bandwidth. While this is adequate for studies of core spatial structure, images with much narrower bandwidth are required for pusher areal density measurements based on x-ray line absorption. For example, measurement of the x-ray line absorption profile through a Ti doped shell requires images within the spectral width of the Ti absorption line (~ 0.1 angstroms).

To satisfy this requirement, we developed a new post-processor code. This code handles the raw data as a stack of one-dimensional images with infinitesimal spectral dispersion (0.008 angstrom/line). The code reconstructs quasi-monochromatic images by sorting and summing many one-dimensional image fragments from a given spectral region of the raw data. The minimum bandwidth obtainable with this method is limited by the spectral resolution of the Bragg mirror ($\lambda/\Delta\lambda$ = 50 - 200 depending on the coating). This technique is essential for reconstruction of narrow spectral-bandwidth images, and provides an alternative reconstruction technique for comparison with earlier approaches [6]. Flexible spectral bandwidth selection in the postprocessor also allows systematic subtraction of the background due to continuum emission. The software also employs a new systematic method of pinhole arrangement estimation as described below.

II. EXPERIMENTAL SETUP

In the experiments, we irradiated the inner surface of the Au hohlraums (inner length: 2.5mm, inner diameter: 1.6mm, diameter of the laser entrance holes: 1.2mm) with 30 beams of the Omega laser [7] (energy: 500 joules/beam, duration: 1ns). The resulting x-rays imploded the plastic capsule (inner diameter: 440 μm, wall thickness 35 μm, filling

gas: deuterium 50 atm. and argon 0.1 atm). To provide spectroscopic diagnostics of shell conditions by absorption of continuum x-ray emission [2], the innermost 3 μm of the capsule wall was doped with Ti (1.6 % in atomic fraction)."

Figure 1 shows the experimental setup of the MMI. A pinhole plate (an array of 1280, 5-μm-diameter pinholes in a 25-μm-thick Ta substrate) is placed 16 mm from an indirectly driven ICF target. A WB_4C Bragg mirror with an interplanar spacing 1.51 nm is placed 82 mm from the target and reflects the images. X-rays satisfying the Bragg condition are projected onto a charge injection device (CID) [8] detector placed 143 mm from the target. The magnification of the system was equal to 8. The spatial resolution of the system was estimated by doing a quadrature sum of the point spread function given by x-ray diffraction through the 5-μm pinholes, geometrical optics (spot size ~ 44 μm on the image plane), and the spatial quantization error due to the pixelated CID detector (38.5-μm pixel interval). The spatial resolution of the system is estimated to be ~7.3 μm on object plane. Figure 2 shows typical raw data, with about 500 images projected onto the CID. There is an approximately linear correspondence between the vertical axis of the raw data and the x-ray wavelength.

III. RECONSTRUCTION PROCEDURE

The code performs background subtraction, spectrum extraction, calibration of spectral dispersion, compensation of spectral sensitivity, estimation of pinhole arrangement, and reconstruction of the quasi-monochromatic images. As a first step, the code subtracts the CID's static background noise from the raw data. The raw data $h(n_x,n_y)$ are then transformed to spatial frequency space $H(k_x,k_y)$ using 2-dimensional fast-Fourier-transform (FFT).

$$H(k_x,k_y)=\sum_{n_x=0}^{N_x-1}\sum_{n_y=0}^{N_y-1}\exp(2\pi ik_x n_x/N_x)\exp(2\pi ik_y n_y/N_y)h\left(n_x,n_y\right) \quad (1)$$

where N_x, N_y are the horizontal and vertical size of the raw data, n_x,n_y and k_x, k_y are the pixel positions in the raw and FFT image. Figure 3 shows the FFT image of Figure 2.

The code extracts a horizontally-integrated vertical profile of the raw data $f(n_y)$ (or photon wavelength spectrum) by executing the inverse Fourier transform as,

$$f(n_y)=\frac{1}{N_y}\sum_{k_y=0}^{N_y-1}\exp(-2\pi ik_y n_y/N_y)H\left(0,k_y\right) \quad (2).$$

As shown on Figure 4, the vertical profile has peaks and dips corresponding to emission lines and absorption lines. The code provides the calibration of the spectral dispersion by fitting the peak positions against the known wavelengths of the lines. The program calculates the effect of non-uniform spectral sensitivity (from the transmission of filters [9], the reflectivity of the Bragg mirror [10], and the sensitivity of the CID [8]) and corrects the spectra accordingly.

The code then sums portions of many individual pinhole images to improve the signal to noise ratio,

$$i(x',y')=\frac{\sum_{j=0}^{N_S(x',y')-1}h(x'+x_j,y'+y_j)}{N_S(x',y')} \quad , (3)$$

where the two dimensional arrays h and i represent the raw and the reconstructed image, (x_j,y_j) is the center position of the j-th image, and $N_s(x',y')$ is the number of fragments summed for the reconstruction of the pixel given by i(x',y'). The image position (x_j,y_j) has to be given accurately in order to avoid distortion and blur in the reconstruction

process. The image position (x_j,y_j) reflects the position and the orientation of the pinhole plate. The pinhole array position varies from shot to shot and cannot be measured *in-situ*. The code therefore estimates the pinhole arrangement by numerically fitting the periodic structure in the raw image. Earlier approaches [6] found the geometrical center of each pinhole image by extracting a center from a family of peripheral contour levels. It is assumed that the peripheral contour levels are dominated by continuum emission and thus are unperturbed by line emissions [6]. The present approach finds center of each image by numerically fitting the periodic structures in the raw data. This procedure is based on the assumption that all pinholes are linearly aligned on the pinhole plate. The high precision of the laser machining technique (+/- 5 μm) allows us to assume the linearity of the pinhole arrangements. The code models the periodic structure with six parameters; the origin (x_0,y_0), the horizontal and the vertical image intervals (D_x, D_y), and the orientation of the rows and the columns of the array (θ,ϕ). A sub-routine generates a periodic reference image g(n_x,n_y) using these parameters,

$$g(n_x, n_y) = A\,(1 + \cos w_x)^2\,(1 + \cos w_y)^2, \qquad (4)$$

where

$$\begin{pmatrix} \omega_x \\ \omega_y \end{pmatrix} \equiv 2\pi \begin{pmatrix} \cos\theta & \sin\theta \\ \cos\phi & \sin\phi \end{pmatrix} \begin{pmatrix} (n_x - x_0)/D_x \\ (n_y - y_0)/D_y \end{pmatrix},$$

and A is an arbitrary constant.

The code evaluates correspondence between the reference image g and the raw data h by,

$$C = \sum_{k_x=1}^{N_x-1} \sum_{k_y=1}^{N_y-1} H(k_x, k_y) G^*(k_x, k_y) \qquad (5)$$

where G* is the complex conjugate of the Fourier transfer of the simulated image g.
The parameters are then optimized to give best correspondence between the reference image and the raw image by maximizing the real part of C and minimizing the imaginary part. We utilized Powell's method [11] for the iterative optimization of the parameters. Because the initial values of the fitting parameters are inferred from the peaks in $H(k_x,k_y)$, Powell's method converges to a unique point without being trapped by local minima. The reconstruction program calculates the image centers (x_j,y_j) in a given spectral range using this optimized parameter set. Quasi-monochromatic images were reconstructed as described by equation (3). Figure 5 shows various quasi-monochromatic images reconstructed from the row data of Figure 2.

Figure 6 (a) shows the lineouts of the reconstructed quasi-monochromatic images shown on fig 5. As shown in fig. 4, the sub-images in band (e) (3.115-3.165 angstrom) and band (g) (3.33-3.38 angstrom) contain not only line emission from the argon tracer but also continuum emission from Bremsstrahlung. The contributions of the continuum emission were estimated by reconstructing images next to the line emission (band (d) 3.065-3.115 and band (f) 3.25-3.30 angstrom). Because both continuum and line emission images are obtained by the same instruments, the contribution of continuum can be subtracted systematically. Figure 6 (b) shows the line profile after continuum subtraction.

In order to check the integrity of the reconstruction process, we analyzed the same raw data with two different codes, the one introduced here and the other reported earlier [6], and found consistent results. The radii of the angle-averaged radial lineout were 14.4, 21.7, and 27.3 μm at 80, 50, and 20% of the maximum intensity the image, respectively. Discrepancies of the radii obtained from the two approaches were within ±1.0 μm.

IV. DISCUSSION

As shown in figure 4, the line emission from the Ar tracer is overlapped on the background emission from continuum, unresolved lines, and satellite lines. These backgrounds have to be subtracted in a two-dimensional manner to obtain pure line transition images.

It is possible to estimate the nearby continuum emission mapping by imaging x-ray emission slightly off the spectral region for the line emission images. For appropriate background subtraction, it is essential to know the spectral sensitivities and effective bandwidths for both the line and the background image.

The MMI has an advantage over bent-crystal imagers in that this background subtraction can be simply performed. The flat Brag mirror provides continuous spectral coverage over a wide spectral range, and the sensitivities for line and background emission are characterized systematically. The postprocessor also allows appropriate bandwidths to be set for image analysis while monitoring the full x-ray spectrum obtained from the same instrument.

In contrast, quasi-monochromatic imaging with bent crystals requires individual x-ray optics for each spectral channel, and at least one channel has to be dedicated for background emission mapping. The subtraction of background emission requires precise characterization of the sensitivities and the effective bandwidths for all channels, and the x-ray spectrum has to be monitored by separate spectrometer.

The images reconstructed with this program show good consistency with those obtained earlier [6]. However, the spectral width of reconstruction can be selected independently from the image size. By reconstructing image with narrow spectral

bandwidths, it is possible to control the vertical spectral dispersion of the reconstructed images.

ACKNOWLEDGEMENTS

The authors acknowledge the support of the staff at the Laboratory for laser Energetics of the University of Rochester. This work was performed under the auspices of the U.S. Department of Energy by the University of California, Lawrence Livermore National Laboratory under contract No. W-7405-ENG-48 and DOE-NLUF Grant No. DE-FG03-03SF22696 to the University of Nevada, Reno. N.I. acknowledges R. E. Turner, Lawrence Livermore National Laboratory, for useful discussions and help with IDL programming.

REFERENCES

[1] I. Golovkin *et al.,* Phys. Rev. Lett 88, 045002 (2002)

[2] V.A. Smalyuk, *et al.,* Phys. Plasmas **10**, 830 (2003).

[3] I. Uschmann, *et al.,* Appl. Opt. **39**, 5865(2000); K. Fujita, et al., Rev. Sci. Instrum. **72**, 744 (2001); Y. Ochi, *et al.,* Rev. Sci. Instrum. **74** 1683 (2003).

[4] F. J. Marshall and Q. Su, Rev. Sci. Instrum. **66**, 725 (1995).

[5] B. Yaakobi, F. J. Marshall, and D. K. Bradley, Appl. Opt. **37**, 8704 (1998); J. A. Koch, *et al.,* Rev. Sci. Instrum. **76** 073708 (2005).

[6] L. A. Welser, *et al.,* Rev. Sci. Instrum. **74**, 1951 (2003).

[7] T. R. Boehly, *et al.,* Opt. Commun. **133** 495 (1997).

[8] F. J. Marshall, *et al.,* Rev. Sci. Instrum. **72**, 713 (2001).

[9] B.L. Henke, E. M. Gullikson, and J. C. Davis, At. Data Nucl. Data Tables 54, 181 (1993).

[10] T. W. Barbee, Lawrence Livermore National Laboratory (private communication).

[11] W. H. Press, S. A. Teukolsky, W. T. Vetterling, B. P. Flannery, *Numerical Recipes in C*, 2nd ed. (CAMBRIDGE UNIVERSITY PRESS, CAMBRIDGE, UK, 1992), pp. 412-420.

FIGURE CAPTION

Fig. 1. Schematic of the experimental set up. The pinhole array projects ~ 500 sub-images onto the CID after reflection by a multi-layer Bragg mirror.

Fig. 2. Typical raw images obtained with the MMI. The images have continuous spectral dispersion along the vertical axis. The bar in the image corresponds to 2 mm at the detector (250 μm on the object).

Fig. 3. Fast Fourier transform of the MMI image. The low frequency region at the center is masked to show weak features in the middle frequency region. The node interval of the grid structure is inversely proportional to the spacing of the sub-images in the raw image.

Fig. 4 X-ray spectrum extracted from raw image of figure 2.

Fig. 5. Quasi-monochromatic images reconstructed from the raw data shown in Fig. 2.: (a) 2.3~2.35 angstrom (below Ti K edge), (b):2.67~2.69 angstrom (within Ti K absorption line), (c)2.75~2.80 angstrom (continuum), (d) 3.065~3.115 angstrom (continuum), (e) 3.115~3.165 angstrom (Ar-Ly-b), (f): 3.25~3.30 angstrom (continuum), (g) 3.33~3.38 angstrom (Ar-He-b), (h) 3.436~3.486 angstrom (continuum). Each image is normalized by its peak value.

Fig. 6. Horizontal lineouts of the reconstructed quasi-monochromatic images on fig. 5. (a) lineout before the continuum subtraction. (b) lineouts after the continuum subtraction.

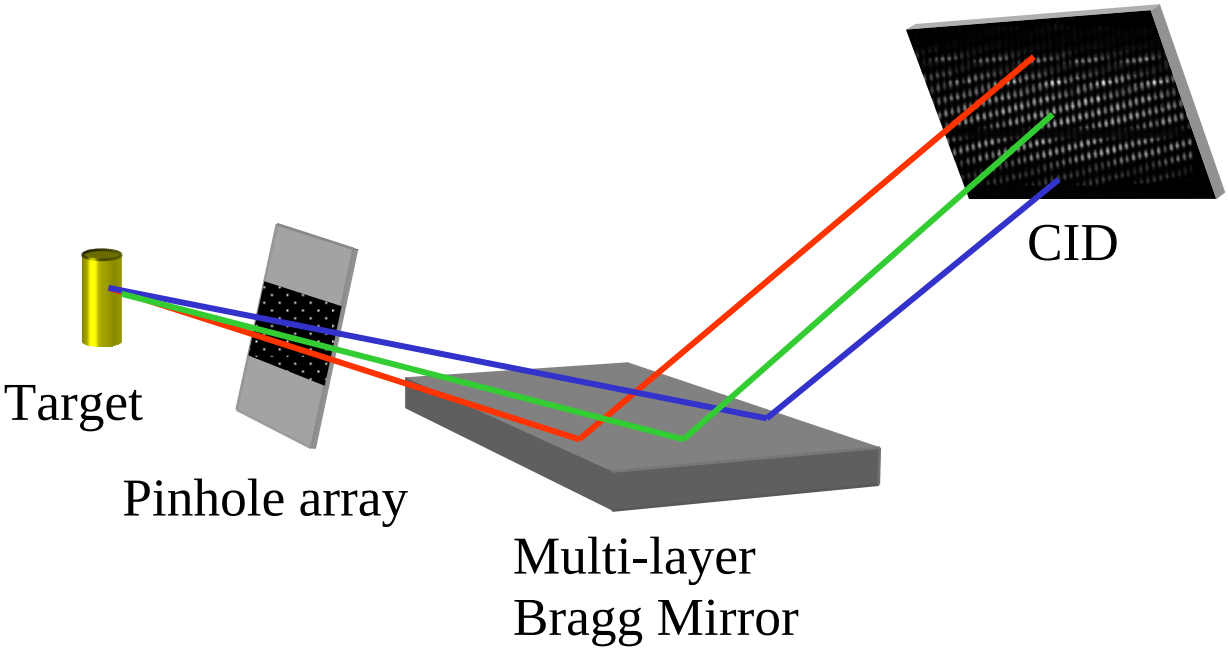

Figure 1

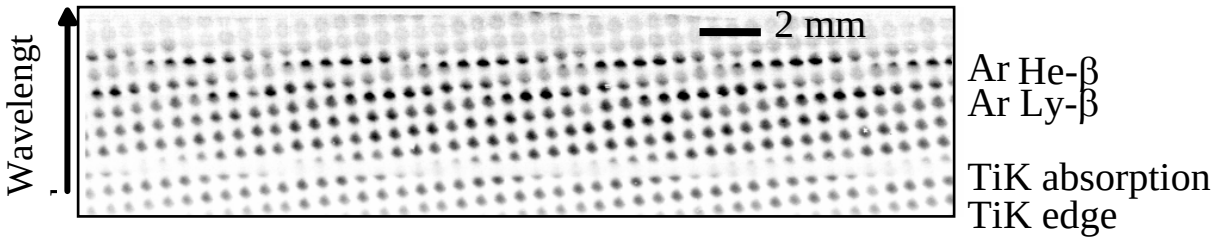

Figure 2

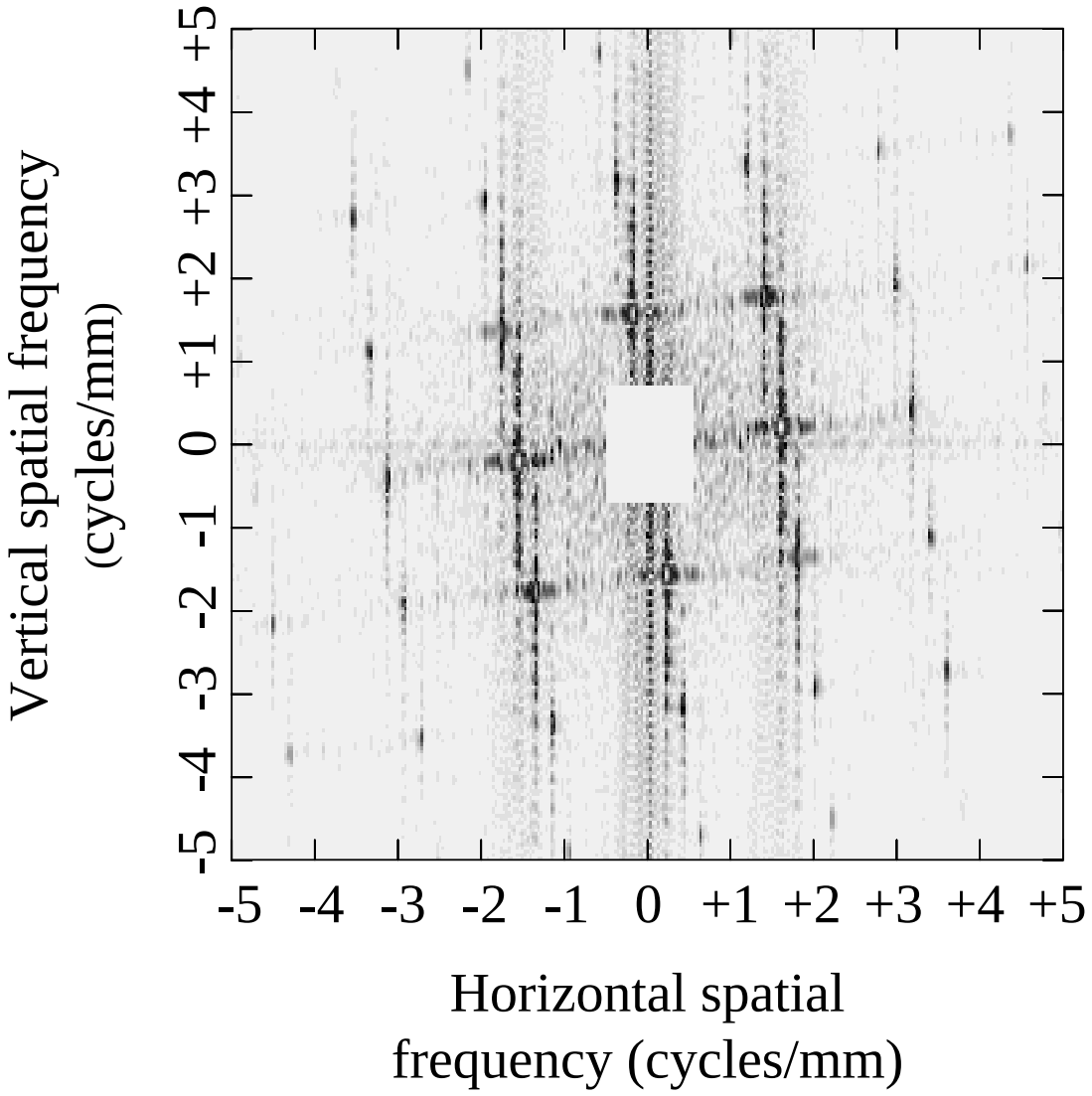
Vertical spatial frequency
(cycles/mm)
-5 -4 -3 -2 -1 0 +1 +2 +3 +4 +5
-5 -4 -3 -2 -1 0 +1 +2 +3 +4 +5
Horizontal spatial
frequency (cycles/mm)

Figure 3

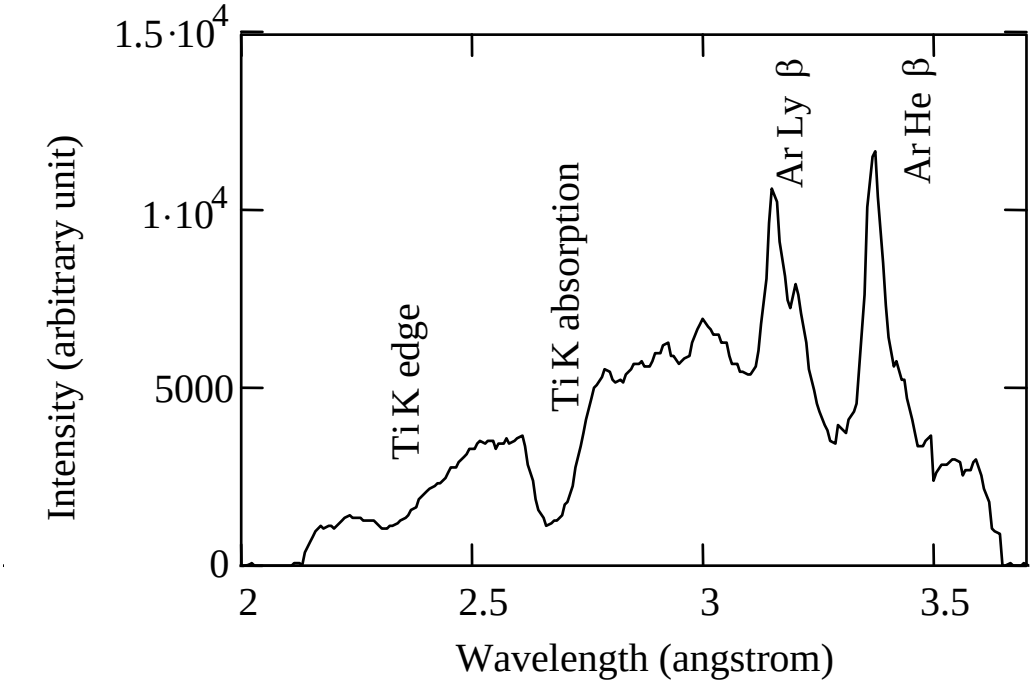
1.5·10^4
1·10^4
5000
0
Intensity (arbitrary unit)
Ti K edge
Ti K absorption
Ar Ly β
Ar He β
2
2.5
3
3.5
Wavelength (angstrom)

Figure 4

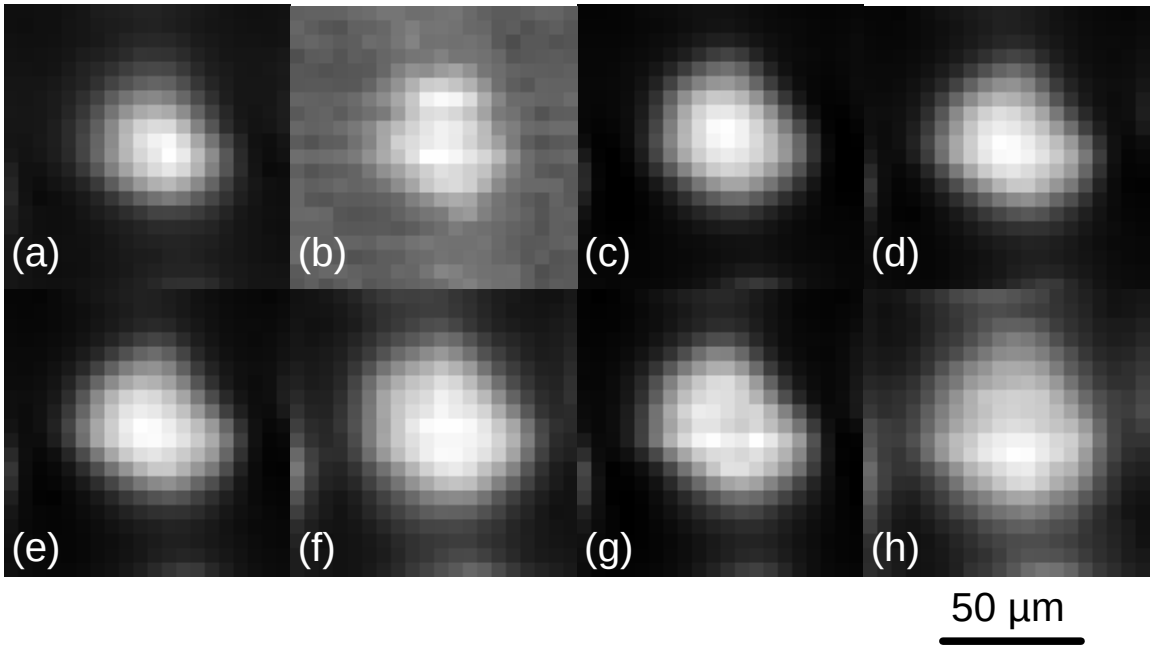

Figure 5

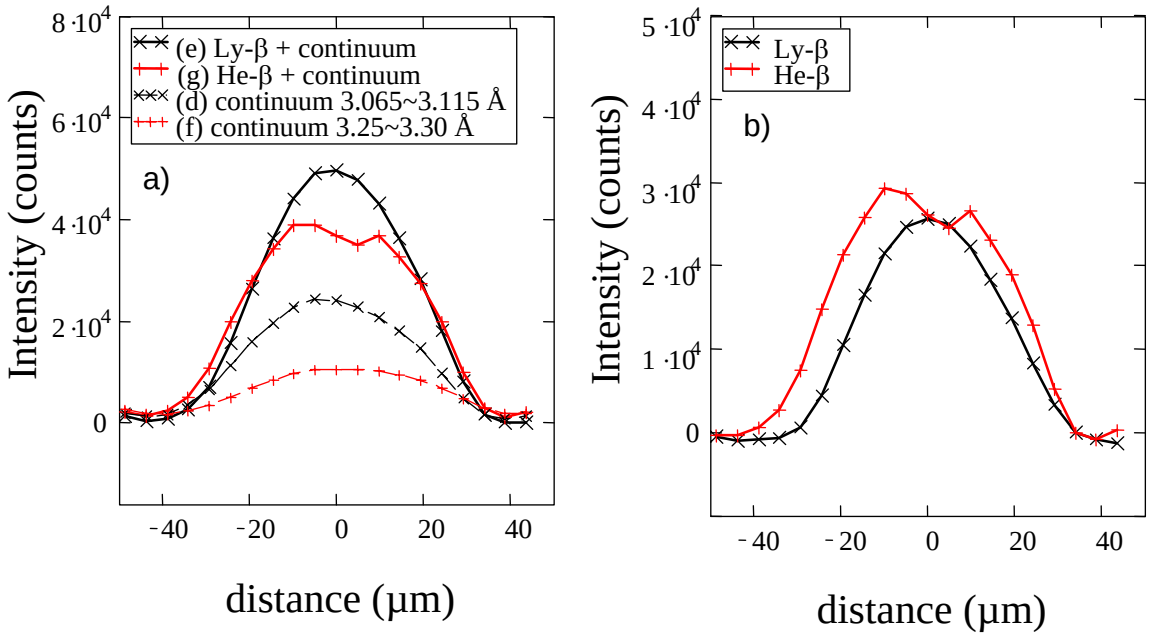
8 ·10^4
6 ·10^4
4 ·10^4
2 ·10^4
0
Intensity (counts)
(e) Ly-β + continuum
(g) He-β + continuum
(d) continuum 3.065~3.115 Å
(f) continuum 3.25~3.30 Å
a)
-40
-20
0
20
40
distance (μm)
5 ·10^4
4 ·10^4
3 ·10^4
2 ·10^4
1 ·10^4
0
Intensity (counts)
Ly-β
He-β
b)
-40
-20
0
20
40
distance (μm)

Figure 6